

Group: Severe Accident Research

JIMEC experiments to investigate jet impingement on a core catcher bottom and LIVE2D 2-Layer experiment

Xiaoyang Gaus-Liu, Thomas Cron, Beatrix Fluhrer, Rene Stängle, Mike Vervoortz, Thomas Wenz

Introduction

In 2019, the research activities in IKET-SAR team were focused on several European projects. Some final work had to be done for the European SAFEST project, coordinated by IKET-SAR team, which ended officially at the end of 2018.

The main activities in 2019 were concentrated on the European ESFR-SMART project. Within this project two large-scale JIMEC experiments have been performed to investigate the thermal ablation kinetics of an internal core catcher material in a SFR reactor. Besides this, the planning work for LIVE-ESFR tests to study the interaction between the corium simulant and the sacrificial simulant of the core catcher started. It has been decided to construct and build a new test vessel with down-scaled geometries similar to SFR core catcher design.

Another activity is the finalization of LIVE2D 2-Layer experimental and analytical analysis, which is a main experimental task in the H2020 IVMR project, which ended in November 2019.

JIMEC experiments to investigate jet impingement on a core catcher bottom and ablation process

Background and Objectives

The actual safety design of a Sodium Fast Reactor (SFR) in the case of a postulated severe accident incorporates to remove the corium from the core by corium transfer tubes and to collect it in the lower head in an in-vessel core catcher. It is assumed that at first a metallic corium melt jet would impinge on the core catcher

surface and could ablate the core catcher material. Experimental data is needed to simulate this ablation behaviour of a long duration melt jet impinging the core catcher material. A particular behaviour can be studied when a molten pool is created ("pool effect") at the impact point that could reduce the heat transfer at the jet – material interface. This phenomenon has been studied very little in the past. Therefore, the IKET-SAR team has adapted the existing MOCKA test facility to perform two JIMEC (Jet Impingement on Metallic Core Catcher) experiments in the frame of the European ESFR-SMART project. JIMEC-1 and JIMEC-2 tests investigate the characteristics of the interaction of a metallic melt jet with the core catcher bottom plate material in a SFR reactor design with prototypical material. The objectives of the experiments are to deliver experimental data on the interaction of melt jet parameter and erosion dynamics. The melt jet parameters were jet temperature, jet velocity and jet diameter. The erosion dynamics in the core catcher bottom is the erosion velocity and the timing of pool effect. The experimental results will be used for developing new correlations which could be used in codes for simulation of the ablation kinetics for SFR core catcher concepts.

Experiments

The two JIMEC experiments have been performed in summer 2019 in the adapted MOCKA test facility, Figure 1. To simulate the core catcher bottom a test substrate was used composed of a cylindrical formed stainless steel block (1.4301) with 416 mm thickness and 425 mm in diameter. A matrix of thermocouples (TCs) was implemented into the test substrate to record the erosion by the melt jet. About 1000 kg of metallic melt was produced by thermite reaction in the separate reaction

crucible above the test substrate. The metallic melt is designed to have the same composition as the metallic test substrate. The outflow opening at the bottom of the crucible was 40 mm in diameter in JIMEC-1 and 30 mm in JIMEC-2. The thermite reaction produced also a lighter oxide melt consisting mainly of Al_2O_3 , Cr_2O_3 and CaO . This melt was redirected by a pouring spout to an oxide melt collector.

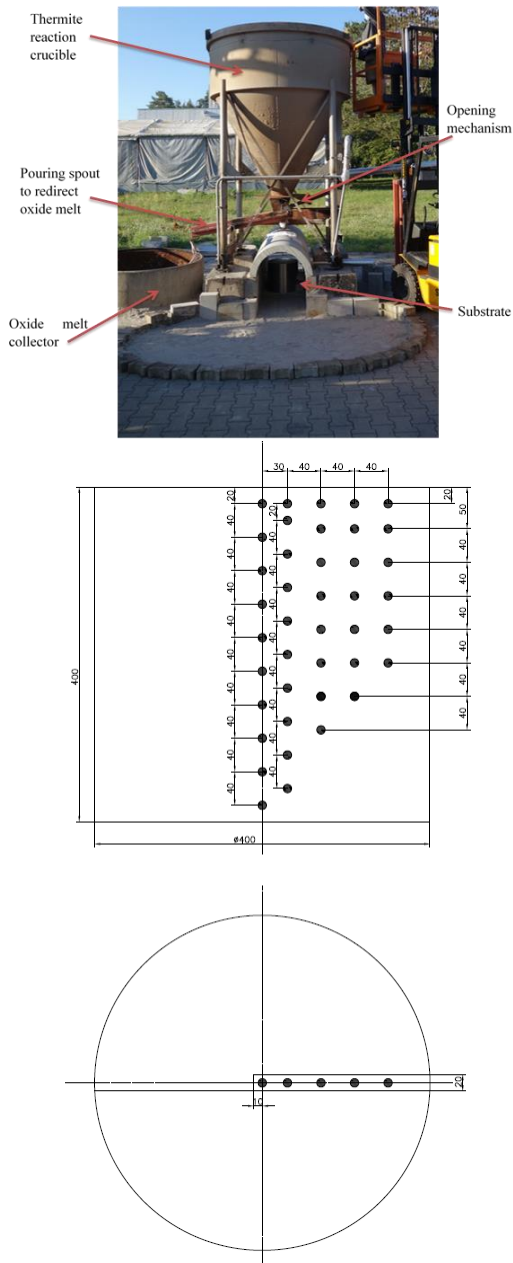


Figure 1: Picture of JIMEC-2 test set-up in top picture and the thermocouple instrumentation in the substrate in the bottom sketch.

For the jet outlet diameter of 40 mm in JIMEC-1, the duration of the metallic melt jet was about 31 s from start of outflow to the end of metallic melt jet. In JIMEC-2 the duration was 55 s due to the smaller jet outlet diameter of 30 mm. In JIMEC-1, the start of pool effect was about 18 s after the first melt reached the substrate indicated by the stop of splashing of the melt, Figure 2. In JIMEC-2, the start of pool effect was detected about 15 s after the first melt reached the substrate surface. Infrared pictures of JIMEC-2 before and after start of pool effect are shown in Figure 3. To protect the environmental apparatus in against the hot splashing melt in JIMEC-2 test, a half-cylinder concrete pipe was positioned upon the substrate with an opening at the jet flow position.

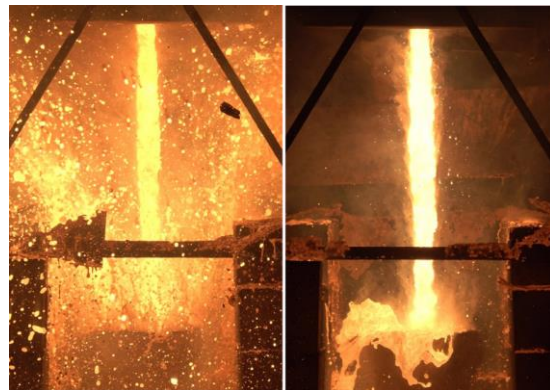


Figure 2: Video pictures of melt jet before and after start of pool effect in JIMEC-1

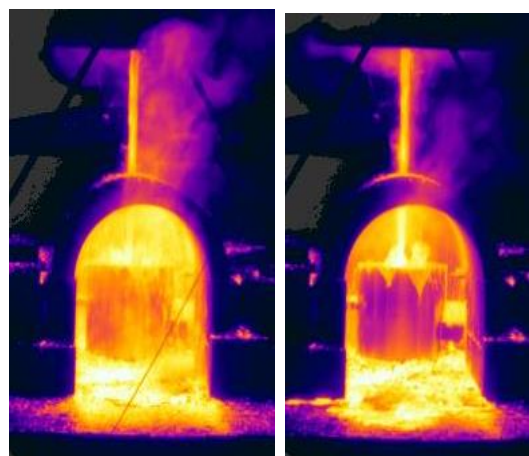


Figure 3: Infrared pictures of JIMEC-2 before and after start of pool effect.

The shape of the jet remained in both tests most time coherent, which means there was no breakup of the jet flow. The jet outflow diameter enlarged during the jet release process since the outlet nozzle made of ZrO_2 was gradually ablated by the metallic and also by the oxide melt. The post-test diameter is 54 – 58 mm for JIMEC-1 and about 46 mm for JIMEC-2. Analysis from high-speed video of JIMEC-1 shows that before the pool effect the melt jet velocity is 4.3 - 4.6 m/s and after the pool effect about 5.0 m/s. The theoretical velocity is about 4.4 m/s at the outlet nozzle. The large velocity at the later phase could be an effect of the enlarged outlet diameter. The metallic melt jet temperature in both tests was in the range of 2000 – 2100 °C measured by a pyrometer. The ablation velocity in the substrate can be obtained based on the thermocouple signals. Figure 4 shows the ablation depth in the substrate versus time for JIMEC-1 and JIMEC-2.

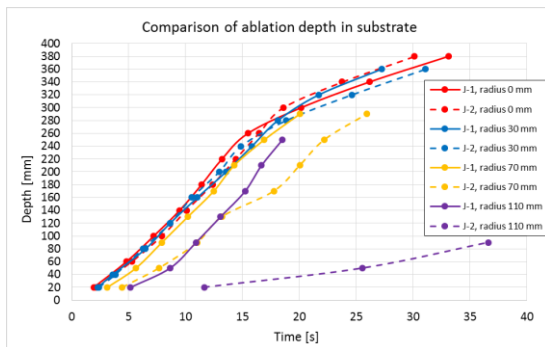


Figure 4: Comparison of ablation depths for JIMEC-1 and JIMEC-2

The ablation rates within 30 mm diameter in the substrate are almost identical for both experiments. The ablation velocity in the center of the substrate is about 17 - 18 mm/s before start of pool effect and decreases to about 7 mm/s after start of pool effect. An influence of the different jet diameter on the ablation behaviour is then detected in the outer regions of the test substrate. For JIMEC-1 with 40 mm jet diameter at the beginning, the radial ablation proceeds faster than for JIMEC-2 with 30 mm jet diameter.

According to the ablation velocity, the contour of ablated pit vs. time can be roughly estimated, as shown in Figure 5. Due to the lacks on measuring position at the outer bottom part, the contour up from 23 seconds can only be partially illustrated. The forms of the contours indicates the initiation of pool effect in 17 sec, leading to a slowdown of the axial ablation, however a high radial erosion rate at the lower part, and thus this led to a gradual transformation of a conic pit to a cylindrical pit.

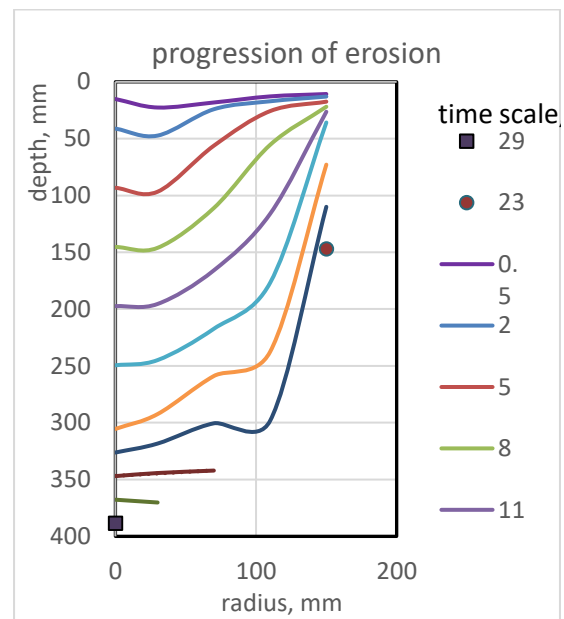


Figure 5: Progression of ablation contour in the JIMEC-1 substrate

The test substrates for JIMEC-1 and JIMEC-2 have been cut after the tests, as shown in Figure 6. The test substrates of JIMEC-1 and JIMEC-2 are molten through by the metallic melt jet. In JIMEC-1 a hole was formed in the lateral wall above a height of ~132 mm from the bottom. Up to the same height, a solidified metal melt has built in the cavity. The mass of both substrates before the tests was about 460 kg. The remaining mass of the test substrate of JIMEC-1 is ~ 240 kg including the solidified metal melt pool. For JIMEC-2, the remaining mass is about 214 kg. Therefore, about 246 kg of the substrate has been molten in IMEC-2 substrate.



Figure 6: Cut of the test substrates of JIMEC-1 and JIMEC-2

Analyses of the LIVE-2D two-layer test series on the heat flux focusing effect and the thermal-hydraulic character in the upper melt layer

Two series of LIVE2D two-layer tests with 3 upper layer thicknesses and different surface boundary conditions were carried out in 2017. The experiment reveals major thermos-hydraulic characteristics of the upper light melt layer during the transient and steady states as well as the strong dependence of the heat flux focusing effect on the upper boundary cooling condition. The final analysis of the two test series comprises the study the heat flux focusing effect upon different boundary conditions and

the characterization of the thermal-hydraulic feature of the upper layer.

Strong heat focusing effect was observed at the wall in the upper melt layer in LIVE2D-SO1 test, which had a hot upper atmosphere. And no heat flux focusing effect appeared when the melt upper surface was rigidly cooled, which was the upper boundary condition of the second test series (LIVE2D-SOTC). Figure 7.

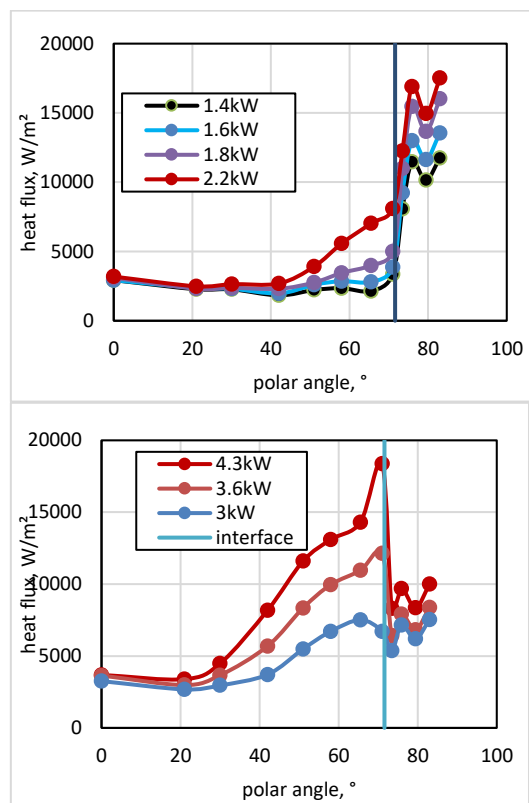


Figure 7: Heat flux at the vessel wall with 110 mm upper layer. Top: during SO1 test; bottom: during SOTC test.

The experiment results demonstrate further that without effective cooling at the upper boundary, the melt circulates globally from the hot central region radially toward the cooled wall boundary, resulting a large diversion of bottom boundary temperature, as shown in Figure 8. Whereas dimensionless temperature $\theta' = (T - T_{min}) / (T_{max} - T_{min})$, z : distance to the bottom and L : the layer thickness. Upon this turbulent flow character, the generally applied Globe&Dropkin correlation, describing convective heat transfer upon a uniform hot

bottom plate to the cold bulk melt in vertical direction, is not suitable for the upper layer heat transfer with limited upper heat transfer rate.

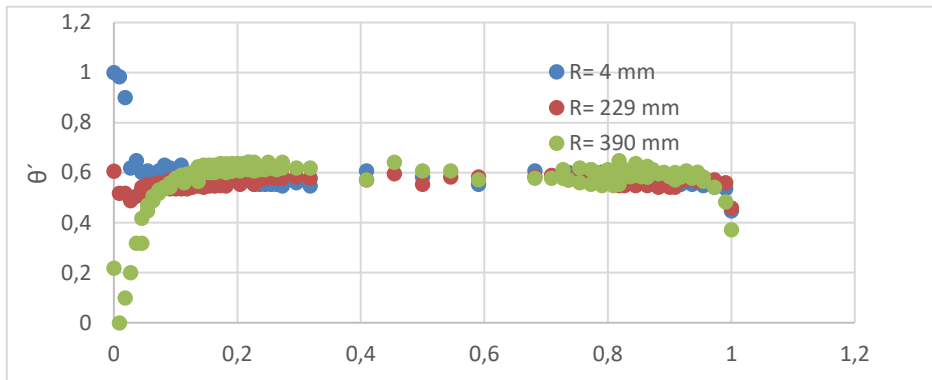


Figure 8: Dimensionless temperature vs. vertical position of a 110 mm upper layer in SO1 test

In addition, the specific boundary combination of the upper layer without strong top cooling doesn't exactly correspond the sidewall heat transfer situation of the widely applied Churchill&Chu correlation, which describes the heat transfer of a heated vertical wall to the cold environment. In Figure 9 the LIVE2D experimental results are plotted in comparison with the two Churchill&Chu correlations, and the experimental results show a considerably lower convective heat transfer capability than the Churchill&Chu correlations.

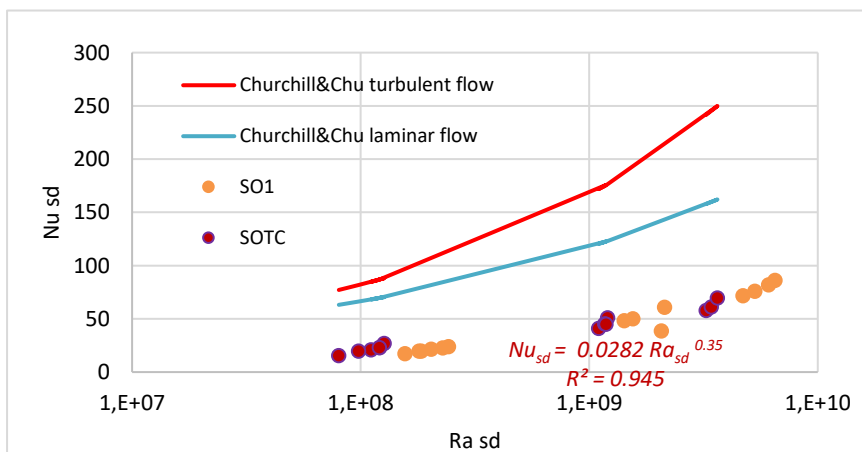


Figure 9: Comparison of Nu at the heat transfer at the upper layer sidewall